Nanoscale

ROYAL SOCIETY OF CHEMISTRY

PAPER

View Article Online
View Journal | View Issue

Cite this: *Nanoscale*, 2025, **17**, 15749

Preparing nitrogen and sulfur-codoped carbon quantum dots to achieve labeling of bovine serum albumin†

Wanqing Li,[a] Xue Chen,[a] Xipeng Dong,[a] Zizhuo Zhai,[a] Yu Kang[b] and Pudun Zhang *[a,b]

Labeling of proteins with carbon quantum dots (CQDs) has always been limited by their complex and cumbersome modifications, which leads to the poor reproducibility of results. In this paper, a one-step solvothermal synthesis approach was developed to prepare nitrogen and sulfur-codoped CQDs using citric acid and thiourea as precursors. Three components emitting blue, yellow and red fluorescence were isolated, and the isothiocyanate functional group was demonstrated to be attached to red emissive CQDs (R-CQDs) by Fourier transform infrared spectroscopy and X-ray photoelectron spectroscopy. Bovine serum albumin (BSA) was successfully labeled with R-CQDs at a mass ratio of 1 : 1 *via* a reaction of the isothiocyanate functional group and the lysine residue of BSA. The labeling of R-CQDs with BSA follows a pseudo-second order kinetic model with a rate constant of 0.0796 h^{-1} and a maximum labeling efficiency of 31.22%. A Förster resonance energy transfer effect was found between BSA and R-CQDs during labeling. The apparent dissociation constant of the R-CQD-labeled BSA and the Hill coefficient are 1.35×10^{-2} mg mL^{-1} and 1.05, respectively, while the binding constant and the number of binding sites are 3.98×10^{2} and 1.35, respectively. This labeling method can also be used for quantification of proteins with a detection limit of 7.0 μg mL^{-1} and is promising to be applied in the integration of optical diagnosis and photothermal therapy due to the outstanding photothermal conversion efficiency (60.6%) of R-CQDs.

Received 25th March 2025,
Accepted 3rd June 2025

DOI: 10.1039/d5nr01242b

rsc.li/nanoscale

1. Introduction

Proteins are commonly labeled before analysis in order to obtain high sensitivity and selectivity. Fluorescent molecules are the most often used reagents for labeling due to their wide variety and availability. Generally, the probe molecule is conjugated to a protein *via* a nucleophilic substitution reaction, in which the specific functional group of the protein with a lone pair of electrons acts as a nucleophile.[1–4] In the case of protein molecules, labeling has to be carried out under mild conditions to prevent protein denaturation, *e.g.*, in water solution at around the physiological temperature and pH. The most commonly labeled functional groups are the sulfhydryl group of cysteine and the ε-amino group of lysine, while maleimide, *N*-hydroxysuccinimidyl esters (NHS) or isothiocyanate (ITC)-modified probes are often adopted because these functional groups have electrophilic centers with high reactivity.

Since lysine residues are abundant in many proteins, ITC-modified fluorescein and rhodamine are among the most used fluorescent labeling reagents. Although such small molecule probes have the advantages of high fluorescence brightness, good specificity and easy operation, they are poor in water solubility and easy to photobleach, and most of them are toxic. Quantum dots (QDs) are a kind of inorganic semiconductor nanomaterial with tunable fluorescence, high quantum yield and excellent photostability. However, they are still poor in water solubility and are toxic due to the use of heavy metal cadmium.[5] Carbon quantum dots (CQDs) are a new type of carbon-based nanomaterial and have received significant attention owing to the wide availability of raw materials, ease of synthesis, outstanding optical properties and good biocompatibility.[6] Currently, CQDs have been utilized in various fields including detection,[7–10] anti-counterfeiting,[11] sensing,[12–15] catalysis,[16] fluorescence imaging,[17,18] photothermal therapy,[19,20] and photoelectric devices.[21,22] In particular, CQDs are well suited for biomedical applications due to their small particle size, rich surface functional groups, excellent photostability, and low cytotoxicity.[23–26]

When being used for the analysis of proteins, CQDs have to be linked *via* a covalent binding or non-covalent adsorption

[a]*College of Chemistry, Beijing University of Chemical Technology, No. 15 Beisanhuan East Road, Chaoyang, Beijing 100029, China. E-mail: zhangpd@mail.buct.edu.cn; Fax: +86 010 64417634; Tel: +86 010 64417634*
[b]*Analysis and Test Center, Beijing University of Chemical Technology, Beijing 100029, China*

† Electronic supplementary information (ESI) available. See DOI: https://doi.org/10.1039/d5nr01242b

strategy while the fluorescence cannot be quenched. The non-covalent adsorption strategy is governed by hydrogen bonding, electrostatic attraction or hydrophobic interaction.[27] This strategy is simple and easy to operate, but such linkage is not secure because desorption might also occur over time, which leads to poor labeling efficiency and reproducibility.[28,29] On the other hand, the covalent binding strategy is similar to that of small fluorescent molecule labeling, which requires functional groups with strong electrophilic active centers on the surface of CQDs to react with proteins. Unfortunately, most of the water soluble CQDs have amino, hydroxyl and carboxyl groups on the surface, which are nucleophilic but have no electrophilic center. Therefore, they cannot react nucleophilically with amino acid residues on proteins. In order to achieve covalent attachment to protein molecules, researchers tried to functionalize the surface of CQDs with electrophilic active centers, among which NHS[28,30–32] and ITC[33,34] are the two most often used compounds because their unparalleled labeling capabilities have been demonstrated by small molecule fluorescent probes. Despite achieving functionalized CQDs with the desired electrophilic groups, the entire procedure is multistep and cumbersome, and the modification yield varies depending on experimental conditions and CQD types, resulting in poor reproducibility of labeling.

Citric acid (CA) and thiourea (TU) are the common carbon, nitrogen (N) and sulfur (S) sources for the synthesis of N,S-codoped CQDs (N,S-CQDs) due to their wide availability and low cost. CA forms the core of CQDs through dehydration, cyclization, aromatization and carbonization at high temperature, while TU tends to form thiocyanate/isothiocyanate (–S–C≡N/–N=C=S) functional groups by deamination. The ammonia produced by decomposition can enter the interior and surface of the core of CQDs to form N-doped CQDs, which are further conjugated with –S–C≡N/–N=C=S groups to generate N,S-CQDs. Based on this knowledge, we prepared N,S-CQDs by a one-step solvothermal method and separated blue, yellow, and red emissive CQDs (B-CQDs, Y-CQDs and R-CQDs) by silica column chromatography, respectively. We found that the surfaces of both B-CQDs and Y-CQDs were functionalized with the –S–C≡N group, while that of R-CQDs was functionalized with the –N=C=S group. Furthermore, the as-prepared R-CQDs were successfully labeled onto BSA without any modification, demonstrating that it is an effective fluorescent probe for protein labeling. Since the obtained R-CQDs also have an excellent photothermal effect, such labeling is promising to be applied in biomedical fields, including the integration of diagnosis and photothermal therapy of major diseases.

2. Materials and methods

2.1 Reagents and materials

CA, TU, *N*,*N*-dimethylformamide (DMF), acetone, dimethylsulfoxide (DMSO), sodium carbonate (Na_2CO_3), sodium bicarbonate ($NaHCO_3$), disodium hydrogen phosphate (Na_2HPO_4) and potassium dihydrogen phosphate (KH_2PO_4) were of analytical grade and used without further purification. Silica (100–120 mesh) was purchased from Qingdao Ocean Chemical Company (China). Bovine serum albumin (BSA, purity ≥98.0%) was purchased from Phygene Life Sciences Company (China). Human serum albumin (HSA, purity ≥99.0%) was purchased from Shanghai EKEAR Bio@Tech Company (China).

2.2 Preparation of N,S-CQDs

N,S-CQDs were prepared by a solvothermal method. Briefly, 1.00 g of CA and 1.98 g of TU (molar ratio of 1/5) were first ultrasonically dissolved in 15.0 mL DMF, and then transferred to a 40 mL Teflon-lined autoclave and reacted at 180 °C for 12 h. After cooling to room temperature, the as-prepared solution was filtered using a 0.22 μm-nylon filter membrane to remove the possible large carbon impurities and then purified by acetone precipitation with a yield of 15% for the crude CQDs. The obtained crude CQD solution was further separated using a home-made silica column. Three components displaying blue, yellow, and red emissions were collected and dried in sequence. Detailed column chromatographic procedures and the obtained chromatogram are given in Note S1 and Fig. S1 in the ESI.†

2.3 Characterization

A Hitachi-7700 transmission electron microscope (TEM) (Hitachi, Japan) with a 200 kV field emission source was used to observe the morphology of CQDs. Fourier transform infrared (FTIR) spectra were recorded with a KBr disc using a Nexus 8700 FTIR spectrometer (Thermo Electron, Madison, WI, USA) with a deuterated triglycine sulfate (DTGS) detector at a resolution of 4 cm^{-1} and 32 co-added scans in the wavenumber range of 4000–400 cm^{-1}. X-ray diffraction (XRD) patterns were obtained using an Ultima IV X-ray diffraction system (Rigaku, Japan) with a Cu K_α radiation source (λ = 0.15418 nm) by scanning from 10° to 70° at an angle interval of 0.02°. X-ray photoelectron spectroscopy (XPS) characterization was performed using an ESCALAB 250 XPS instrument (Thermo Fisher Scientific, USA) with a monochromatic Al K_α radiation source (150 W) and a spot size of 500 μm. Ultraviolet-visible (UV-vis) absorption spectra were recorded using a UV-3600 spectrophotometer (Shimadzu, Japan). Fluorescence spectra were recorded using an F-7000 fluorescence spectrometer (Hitachi, Japan) at a PMT voltage of 800 V with slit width of 5 nm for both excitation and emission. Both the absolute quantum yields (QYs) and fluorescence decay curves were measured using an FLS 980 steady-state/transient spectrometer (Edinburgh Instruments, UK). Photothermal curves of R-CQDs were recorded using an infrared thermal imaging system (FLIR-A600-Series, Sweden) by irradiating an 808 nm diode laser with fiber optics on the solution at a distance of 1 cm.

2.4 Labeling of BSA with R-CQDs

The labeling procedure of BSA with R-CQDs is similar to that with FITC, as reported elsewhere.[35,36] Briefly, BSA and dried

R-CQD powder were first dissolved in Na_2CO_3–$NaHCO_3$ buffer (pH 9.0) and DMSO at a concentration of 1.0 mg mL^{-1}, respectively. Then 1.0 mL of the R-CQDs solution was added dropwise to an equal volume of BSA solution under shaking. The mixture was vortexed and incubated at room temperature for varied durations (0.5 h, 1 h, 1.5 h, 1.7 h, 2 h, 3 h, and 6 h). After incubation, each mixture was separated using a home-made Sephadex G-50 gel column and eluted with phosphate-buffered saline (PBS) solution (pH 7.4). The labeled protein could be easily distinguished from the eluent by the naked eye because this section had a distinct purple color. Finally, the obtained R-CQD-labeled BSA (R-CQDs@BSA) solution was concentrated using a Millipore ultrafiltration tube (MWCO = 30 000) and the volume was fixed to 1.0 mL. The optimal R-CQDs concentration for labeling and the maximum amount of BSA that can be labeled were achieved by changing their respective concentrations.

3. Results and discussion

3.1 Optical, morphological and chemical characterization of N,S-CQDs

Since the UV absorption and fluorescence emission spectra of crude CQDs show three absorption peaks and three independent emission peaks (Fig. S2a and b†), it is suggested that there might exist three luminescent centers in the N, S-CQDs, as pointed out in the literature,[37] or it might be a mixture of three independent CQDs. To confirm which one is correct, column chromatography was used to purify the obtained crude CQDs, and three components emitting blue, yellow and red fluorescence were obtained (Fig. S1†). Only one excitation-independent emission peak is observed for each component (Fig. S3a–c†), demonstrating that the crude N,S-CQDs are a mixture of B-CQDs, Y-CQDs and R-CQDs. This result is different from the literature,[37] in which the authors considered that there are three luminescent centers in the N,S-CQDs prepared by the similar conditions to us. The reason for this might be that they purified the CQDs just by precipitation and without any chromatographic procedure, which led to the three components not being able to separate.

It is shown from Fig. 1a–c that two absorption peaks at 260 nm and 350 nm appear in the UV spectra of the three CQDs, which are attributed to the π–π* transition of aromatic sp^2 C=C and the n–π* transition of C=O and/or C=N, respectively. In addition to these two common peaks, Y-CQDs also display an absorption peak at 440 nm, while R-CQDs exhibit two absorption peaks at 515 nm and 545 nm. The appearance of long-wavelength absorption peaks is due to the formation of a larger aromatic conjugated structure and the doping of heteroatoms that can form the chromophores (*e.g.*, C=O, C=N, C=S, *etc.*) or auxochromes (*e.g.*, OH, NH_2, SR, *etc.*) on surface of CQDs.[37,38] Besides, it is also shown that both the fluorescence excitation and emission wavelengths are red-shifted from 370/445 nm ($\lambda_{ex}/\lambda_{em}$) (B-CQDs) to 445/545 nm (Y-CQDs) and further to 550/605 nm (R-CQDs). Such a color change of the three N,S-CQDs solutions can also be visually observed under daylight and an ordinary flashlight with near-UV (365 nm), blue and green light, respectively, as shown in the insets of Fig. 1a–c. The high overlap of absorption and excitation peaks indicates the existence of surface state luminescence.[39] In addition, the average lifetimes of 6.92 ns, 6.20 ns and 4.85 ns for the aqueous B-CQD, Y-CQD and R-CQD solutions are obtained from their respective fluorescence decay curves (Fig. 1d–f), in which the contributions of τ_2 are much larger than that of τ_1. Since τ_1 and τ_2 are caused by the non-radiation transition of the intrinsic state and the surface defects,[40] respectively, the results also suggest a surface state luminescence mechanism. At their optimal excitation wavelengths, the absolute fluorescence QYs of B-CQDs, Y-CQDs, and R-CQDs are 12.3%, 8.5%, and 7.4%, respectively. Furthermore, the fluorescence stability of the three CQDs was evaluated in terms of their salt and pH tolerance as well as preservation and continuously long-time irradiation. The results (Fig. S4†) indicate that the three CQDs exhibit outstanding photostability, anti-bleaching and robust environmental resilience, which paves the way for their potential applications in a number of fields.

Nevertheless, considering the fact that R-CQDs have relatively low fluorescence QYs and the absorption curve shows an obvious increase in the range of 600–850 nm (Fig. S5†) with an extinction coefficient of 1.29 L g^{-1} cm^{-1} at 808 nm, it is rationally presumed that most of the absorbed energy in long wavelengths might be converted into thermal energy through non-radiative relaxation. Therefore, the photothermal effect of R-CQDs was also investigated using an approach similar to those presented in the literature.[41,42] As shown in Fig. S6,† a rather high photothermal conversion efficiency (PCE) of 60.6 ± 0.7% (n = 3) was achieved for R-CQDs, validating the presumption. The excellent photothermal effect provides an opportunity for R-CQDs in biomedical applications. For instance, it is promising to be used in photothermal diagnosis and therapy of tumor *via* selectively labeling R-CQDs with proteins.

The TEM images (Fig. 1g–i) demonstrate that the three individual N,S-CQDs are quasi-spherical particles with average diameters of 2.84 nm (B-CQDs), 3.60 nm (Y-CQDs) and 5.13 nm (R-CQDs), respectively. The gradual increase of the particle size from B-CQDs to Y-CQDs and further to R-CQDs indicates that the quantum confinement effect also contributes to the luminescence of the as-prepared N,S-CQDs in addition to the surface state. Besides, a broad peak at 27.2° is observed in the XRD patterns of the three CQDs (Fig. S7†), which is attributed to the diffraction of the (002) plane of the graphitic structures of CQDs.[38] Due to the dispersion of the smaller particle size, B-CQDs display a broader and weaker diffraction peak than Y- and R-CQDs.

The FTIR spectra (Fig. 2) suggest similar chemical structures of the three CQDs. In particular, there exist hydroxyl (3420 cm^{-1}), amino (3210 cm^{-1}), alkyl (2976 and 2850 cm^{-1}), thiocyanoate/isothiocyanate (2062/2074 cm^{-1}), imide (1770

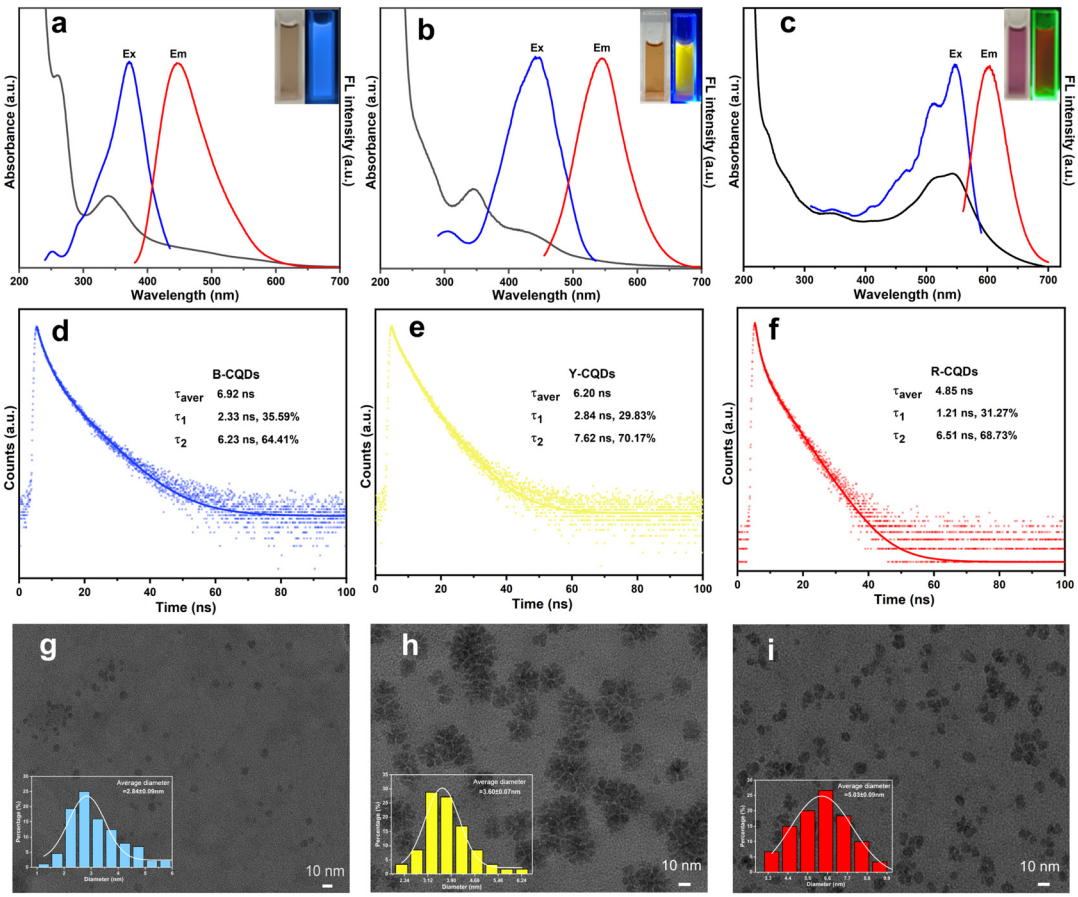

Fig. 1 (a–c) UV–vis absorption (black), excitation (blue) and emission spectra (red) of B-CQDs, Y-CQDs and R-CQDs, respectively. The insets of (a–c) show the photos of the three CQD aqueous solutions under irradiation of daylight and ordinary flashlight with near-UV (365 nm), blue and green light. (d–f) Fluorescence decay curves of B-CQDs, Y-CQDs and R-CQDs, respectively. The insets of (d–f) are the average lifetimes (τ) and the contributions of τ_1 and τ_2. (g–i) TEM images of B-CQDs, Y-CQDs and R-CQDs, respectively. The insets of (g–i) show the particle size distribution histogram of each.

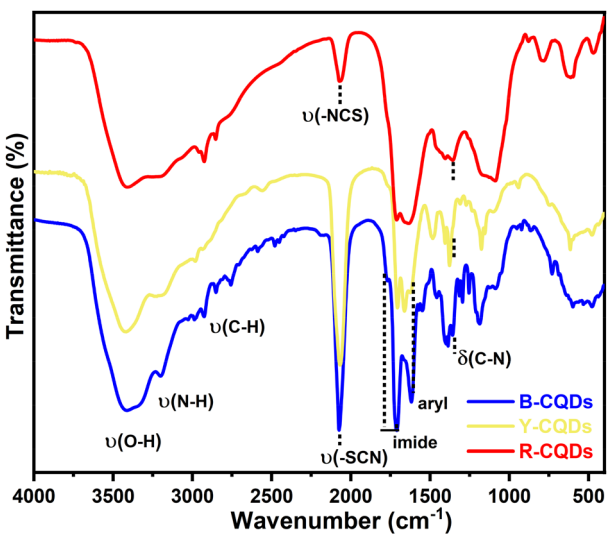

Fig. 2 FTIR spectra of B-CQDs, Y-CQDs and R-CQDs.

and 1705 cm^{-1}), and aryl (1618 and 775–730 cm^{-1}) groups on the three CQDs. Nevertheless, some differences in the chemical structures are still found amongst them. (1) The strong absorption band at 2062 cm^{-1} of B-CQDs and Y-CQDs is mainly caused by the –S–C≡N group, while the relatively weak band at 2074 cm^{-1} of R-CQDs is attributed to the –N=C=S group. However, the elemental analysis result (Table S1†) shows that the amounts of sulfur (S) gradually increase from B-CQDs to Y-CQDs and further to R-CQDs, indicating that considerable amounts of S are converted into other S-containing functional groups as carbonization proceeds. (2) The band intensities of the imide group (1770 and 1705 cm^{-1}) also decrease from B-CQDs to Y-CQDs and further to R-CQDs, though it is not very obvious. The imide group can be cleaved into an amide group (1662 cm^{-1} in the FTIR spectrum of Y-CQDs) and further carbonized into pyrrolic or pyridinic structures (1620 cm^{-1} in the FTIR spectrum of R-CQDs). Such a result is also illustrated by the increase of the C–N bending vibration band (δ_{C-N}) intensity at 1352 cm^{-1}.

The XPS survey scans (Fig. 3a) display the presence of C (285 eV), N (400 eV), O (532 eV), and S (164 eV) elements on the three CQDs. The high-resolution C 1s spectra (Fig. 3b) show three Gaussian peaks at 284.4 eV, 285.6 eV and 288.0 eV, corresponding to the C–C/C═C (sp^2 C), C–O/C–N (sp^3 C) and C═O/C═N groups, respectively. It is noticed that the contents of the C═O/C═N bonds of Y-CQDs and R-CQDs are larger than that of B-CQDs, indicating that more heteroatom-doped carbon cores were formed. Similarly, three N species, including pyridinic N (398.8 eV), pyrrolic N/amino N (399.6 eV) and graphitic N (401.2 eV) are identified from the high-resolution N 1s spectra (Fig. 3c) and the content of graphitic N gradually increases from B-CQDs to Y-CQDs and further to R-CQDs. The increase in the content of graphitic N narrows the HOMO–LUMO gap and therefore favors the redshift of emission.[43,44] Likewise, the high-resolution O 1s spectra (Fig. 3d) signify the presence of C═O (531.2 eV) and C–O (533 eV) groups, respectively, and the increase of the C═O group also leads to a red-

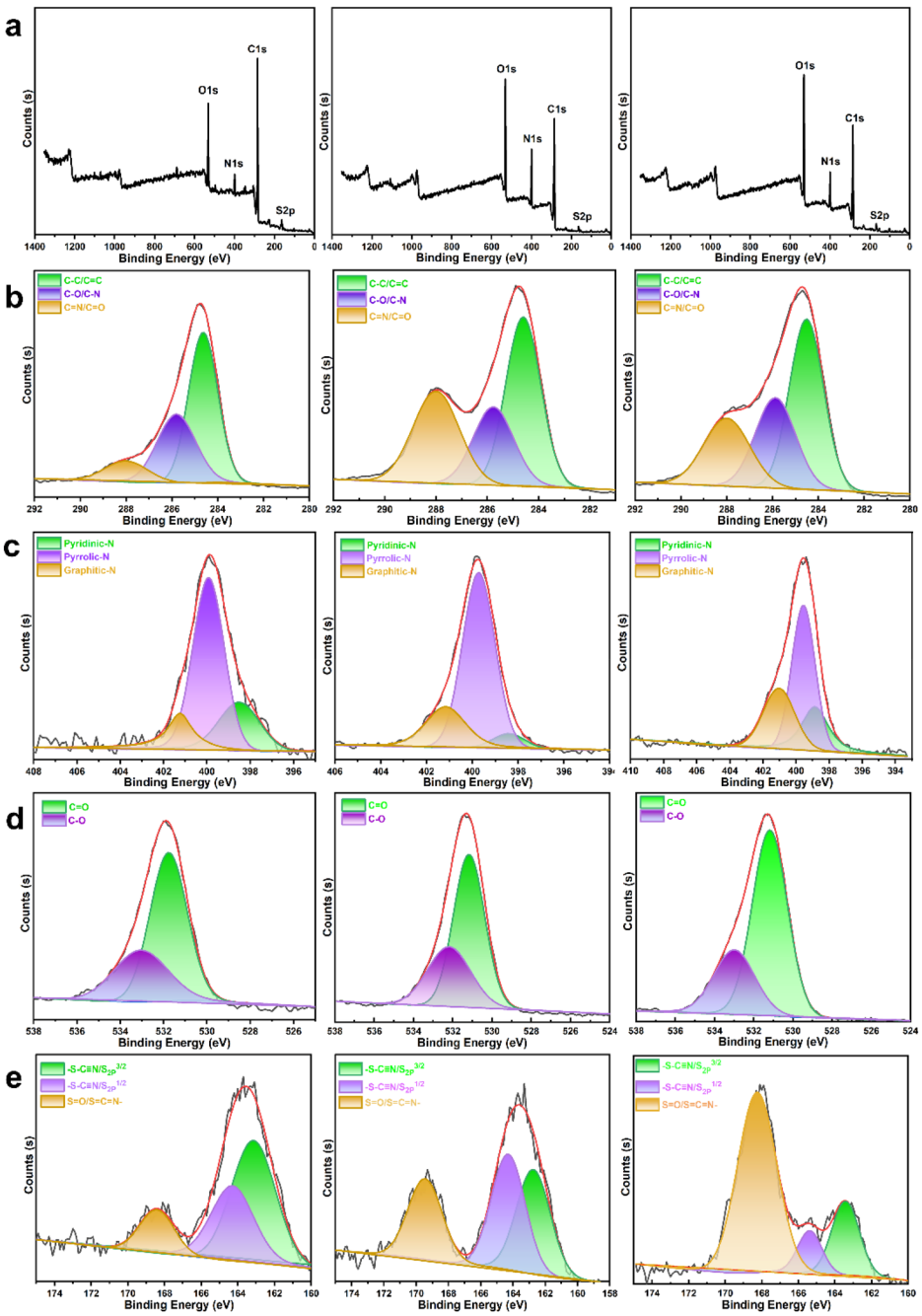

Fig. 3 (a) XPS survey scans of B-CQDs (left column), Y-CQDs (middle column) and R-CQDs (right column). (b–e) High-resolution C 1s, N 1s, O 1s and S 2p XPS spectra of B-CQDs, Y-CQDs and R-CQDs.

shift of emission.[43] In addition, three peaks located at 162.8–163.3 eV, 164.2–165.4 eV and168.2–169.4 eV are observed in the high-resolution S 2p spectra (Fig. 3e). The former two peaks correspond to the S $2p^{3/2}$ and S $2p^{1/2}$ states of the C–S bond, respectively, which might be caused by the thiophene or thiazole structure, while the latter corresponds to the –N═C═S group, which was demonstrated by FTIR. The identification of the –N═C═S and –S–C≡N groups can be confirmed by using fluorescein isothiocyanate (FITC) and KSCN, as shown in Fig. S8.† The possible formation mechanism of the thiocyanate or isothiocyanate group on the N, S-CQDs are given as Note S10 in the ESI.†

3.2 Interaction between R-CQDs and BSA

Although the fluorescence QYs of both B-CQDs and Y-CQDs are larger than that of R-CQDs, there are more –N═C═S functional groups on the surface of R-CQDs based on FTIR and XPS results, which suggest that R-CQDs can be directly used for protein labeling without any additional modification according to a nucleophilic reaction mechanism (Note S11 in the ESI†). For this reason, BSA and R-CQDs were treated according to the procedure given in section 2.4. The UV spectrum of the resulting product contains the spectral features of both BSA and R-CQDs (Fig. 4a), confirming that R-CQDs had been successfully labeled onto BSA.

It is well known that BSA has an intrinsic fluorescence at 340 nm, which is susceptible to the molecules around BSA. Therefore, the interaction between BSA and R-CQDs has to be investigated before establishing the labeling method. By fixing the concentration of one and increasing the concentration of the other, a series of fluorescence emission spectra are obtained under excitation at 280 nm and 550 nm, respectively, and the influence of each on the fluorescence intensity of the other can therefore be studied. As depicted in Fig. 4b, when varied concentrations of R-CQDs were added in BSA solutions (maintaining the concentration of BSA at 0.1 mg mL^{-1}), the intrinsic fluorescence intensity of BSA at 340 nm shows a significant decreasing trend. On the other hand, when varied concentrations of BSA were added to R-CQD solutions (maintaining the concentration of R-CQDs at 0.1 mg mL^{-1}), the fluorescence intensity of R-CQDs displays an increasing trend with a slight redshift of the emission center (Fig. 4c). It is noticed that the addition of R-CQDs resulted in a decrease in the intrinsic fluorescence of BSA until it was completely quenched, but in turn, the fluorescence of R-CQDs was enhanced due to adding BSA. These interesting phenomena indicate that Förster resonance energy transfer (FRET) might occur between BSA and R-CQDs during labeling, which can be substantiated by the significant spectral overlap (Fig. S9†) between the emission spectrum of BSA (donor) and the absorption spectrum of R-CQDs (acceptor).[45] In addition, the decrease of the average fluorescence lifetime of BSA from 5.55 ns to 4.56 ns before and after labeling of R-CQDs (Fig. 4d) also confirms the FRET effect. Furthermore, the dependence of the fluorescent signal of BSA on the R-CQD concentration was investigated using the Hill model (see Note S13 in the ESI† for details),[45–49] and the ratio of the fluorescence intensity (F^*) of BSA at 340 nm to that of initial BSA *versus* the concentration of added R-CQDs is shown in Fig. 4e. The apparent dissociation constant (K'_d) and the Hill coefficient (h) are 1.35 × 10^{-2} mg mL^{-1} and 1.05,

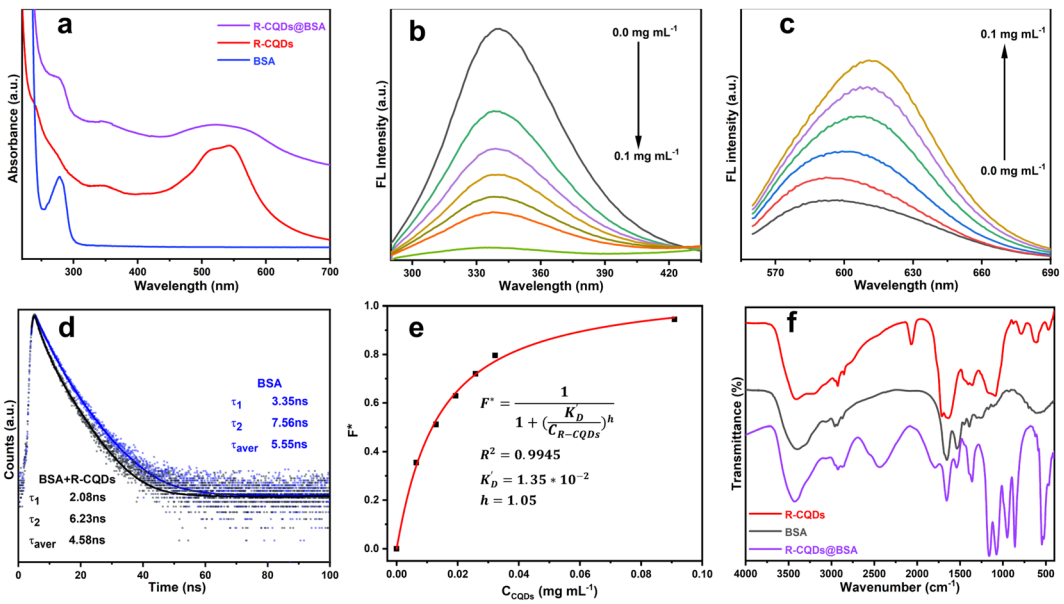

Fig. 4 (a) UV-vis absorption spectra of R-CQDs, BSA and R-CQDs@BSA. (b) Fluorescence spectra of BSAs after adding increasing concentrations of R-CQDs under excitation at 280 nm. (c) Fluorescence spectra of R-CQDs after adding increasing concentrations of BSAs under excitation at 550 nm. (d) Fluorescence decay curves of BSA and R-CQDs@ BSA. (e) Plot of the ratio of the fluorescence intensity (F^*) of BSA at 340 nm to the one of initial BSA *versus* the concentration of added R-CQDs according to the Hill equation (Note S13 in the ESI†). (f) FTIR spectra of R-CQDs, BSA and R-CQDs@BSA.

respectively, indicating a weak positive cooperativity of interaction between R-CQDs and BSA. The reaction between BSA and the –N=C=S group of R-CQDs can also be validated by FTIR. As shown in Fig. 4f, the absorption band of the –N=C=S group (2074 cm^{-1}) disappears after labeling and instead a C=S characteristic band appears at 1360 cm^{-1}. Note that the bands less than 1250 cm^{-1} in the spectrum of R-CQDs@BSA are caused by the phosphate used for elution. The FTIR results demonstrate that the interaction between BSA and R-CQDs is not a simple adsorption but forming a new chemical group (substituted thiocarbamide). Apart from these, a binding equilibrium constant of BSA with R-CQDs (K = 3.98 × 10^2) and the number of binding sites (1.35) can also be determined by quenching the fluorescence of BSA,[49] which is discussed in detail in Note S14 and Fig. S10 (ESI†). This result is in good agreement with that calculated from the Hill model for the dissociation coefficient (K_D). The developed R-CQDs in this work not only exhibit similar specificity and stability to the conventional multi-step functionalized CQDs, but also possess higher labeling efficiency and reproducibility. Moreover, the specificity of labeling can be significantly enhanced by linking R-CQDs to a special antibody, and then utilizing the specific interaction between the antibody and the antigen.

3.3 Labeling of BSA with R-CQDs

As discussed in section 3.2, BSA can be successfully labeled with R-CQDs through a covalent conjugation. Generally, the absorbance at 280 nm is applied to quantify the concentration of proteins using an external standard method based on the Beer–Lambert law. However, an obvious absorption at this wavelength is also observed in the UV spectrum of R-CQDs, leading to an elevated apparent absorbance at 280 nm when they are conjugated. As a result, an artificially high BSA concentration would be achieved compared to the true concentration when an external standard method is adopted; therefore, a correction procedure has to be studied. Note that R-CQDs have an absorption at 350 nm while BSA does not show any absorption (Fig. 4a), the absorbance at this wavelength would not be influenced by BSA when they are conjugated and is therefore chosen as the reference to correct the contribution of R-CQDs to the apparent absorbance at 280 nm. The correction factor (CF) is defined as:

$$\mathrm{CF} = \frac{A_{280}^{\mathrm{CQDs}}}{A_{350}^{\mathrm{CQDs}}} \quad (1)$$

where A_{280}^{CQDs} and A_{350}^{CQDs} represent the absorbance of pure R-CQDs at 280 nm and 350 nm, respectively. According to the definition, a determination procedure is given in Note S15 and Fig. S11 (ESI†) and a CF of 1.27 was thus obtained.

Consequently, the true absorbance of labeled BSA ($A_{280}^{\mathrm{BSA*}}$) can be calculated by

$$A_{280}^{\mathrm{BSA*}} = A_{280}^{\mathrm{CQDs@BSA}} - \mathrm{CF} \times A_{350}^{\mathrm{CQDs@BSA}} \quad (2)$$

where $A_{280}^{\mathrm{CQDs@BSA}}$ and $A_{350}^{\mathrm{CQDs@BSA}}$ represent the apparent absorbance of R-CQDs@BSA at 280 nm and 350 nm, respectively. Furthermore, the labeling efficiency (LE) of BSA using R-CQDs can also be calculated by

$$\mathrm{LE} = \frac{A_{280}^{\mathrm{BSA*}}}{A_{280}^{\mathrm{BSA^0}}} \times 100\% = \frac{A_{280}^{\mathrm{CQDs@BSA}} - \mathrm{CF} \times A_{350}^{\mathrm{CQDs@BSA}}}{A_{280}^{\mathrm{BSA^0}}} \times 100\% \quad (3)$$

where $A_{280}^{\mathrm{BSA^0}}$ represents the absorbance of BSA at its initial concentration.

In order to achieve an optimal labeling, the reaction time, the concentration of R-CQDs, and the maximum concentration of labeled BSA were investigated. It is shown in Fig. 5a that labeling was already finished within two hours. Fig. S12† also displays that the fluorescence intensity of the labeled BSA reaches the maximum after two hours, further evidencing the results of UV absorption. The inset of Fig. 5a shows an excellent linearity between t/LE_t and t (R^2 = 0.9907), suggesting that the labeling of BSA with R-CQDs follows the pseudo-second-order kinetic model

$$\frac{t}{\mathrm{LE}_t} = \frac{1}{k\mathrm{LE}_e^2} + \frac{t}{\mathrm{LE}_e} \quad (4)$$

where LE_t is the labeling efficiency at any time t, LE_e is the one at which the maximum labeling is reached, and k is the rate constant. In this case, the labeling rate constant (k) of 0.0796 h^{-1} and the maximum LE (LE_e) of 31.22% can be achieved from the fitting parameters given in the inset of Fig. 5a. Next, the influence of R-CQD concentration on LE was investigated and the maximum LE is obtained at 1.0 mg mL^{-1} (Fig. 5b). Finally, a maximum concentration of 1.024 mg mL^{-1} for the labeled BSA (*i.e.*, R-CQDs@BSA) can be obtained by examining the reaction of different concentrations of BSA with 1.0 mg mL^{-1} of R-CQDs for 2 hours (Fig. 5c), indicating that BSA reacted with R-CQDs at a mass ratio of 1 : 1 when labeling reached the maximum. It is noticed that a good linearity is found when the BSA concentration is less than 4.0 mg mL^{-1}, suggesting that R-CQDs can be applied for quantification of proteins. To validate this, 1.0 mg mL^{-1} of R-CQDs was used to label a series of BSA solutions with varied concentrations, and then the fluorescence spectrum of each R-CQDs@BSA was recorded (Fig. 6a). An excellent linearity between the fluorescence intensity and the BSA concentration is achieved (Fig. 6b) with a limit of detection (LOD) of 7.0 μg mL^{-1}. Similarly, human serum albumin (HSA) was also successfully labeled with R-CQDs using this developed approach, and a good linearity can also be obtained (Fig. S13a–c†).

In addition, in order to investigate the influence of light on LE, labeling was implemented under the same conditions (2 h, 1.0 mg mL^{-1}) under daylight, dark and UV irradiation at 365 nm, respectively. The results (Fig. S14†) show that both the LE and fluorescence intensity of R-CQDs@BSA remain virtually unchanged, indicating that light has no influence on labeling.

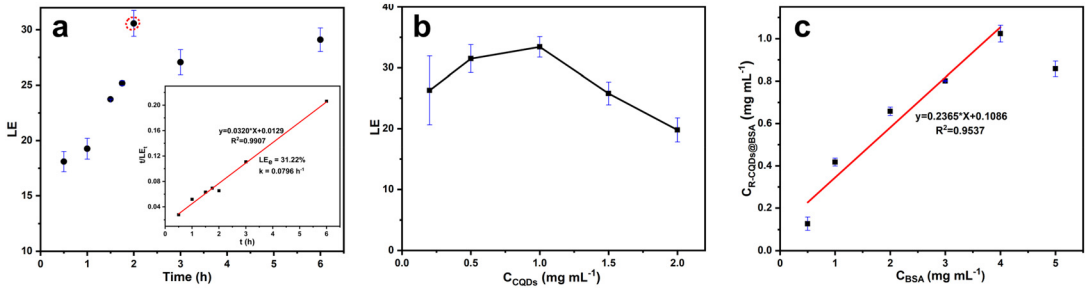

Fig. 5 (a) Relationship between the labeling efficiency (LE) and the time. The inset shows a linear relationship between t/LE_t and the time (t). (b) Effect of the R-CQDs concentration on LE. (c) Relationship between the R-CQDs@BSA concentration and the added BSA concentration; a good linearity is achieved in the BSA range of 0.0–4.0 mg mL^{-1}.

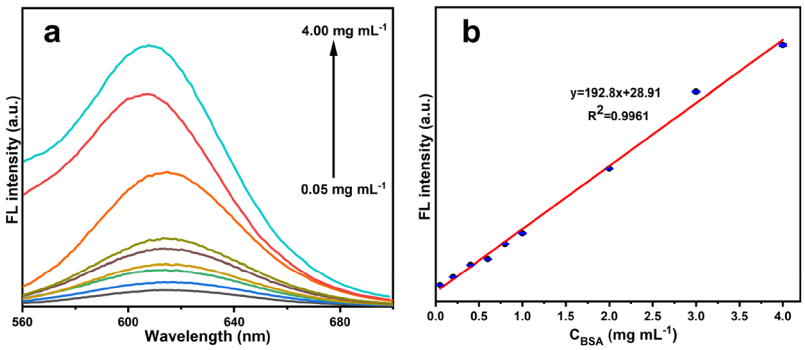

Fig. 6 (a) Fluorescence spectra of BSA with varied concentrations (0.05–4.0 mg mL^{-1}) labeled with 1.0 mg mL^{-1} of R-CQDs. (b) Relationship between the fluorescence intensity and the BSA concentration.

4. Conclusions

In summary, a one-step solvothermal synthesis method to prepare N,S-codoped CQDs was developed by using CA and TU as precursors, and the CQDs emitting blue, yellow and red fluorescence were isolated by silica column chromatography. The optical and morphological characterization studies demonstrated the synergetic luminescence effects of the surface state and quantum confinement. Interestingly, the FTIR and XPS results showed that the isothiocyanate functional group (–N=C=S group) was attached to the surface of R-CQDs, while the thiocyanate functional groups (–S–C≡N) were attached to the surfaces of both B-CQDs and Y-CQDs. To the best of our knowledge, this work is the first reported one in which the reactive functional groups were linked to CQDs without additional complex reactions. Based on this feature, R-CQDs were successfully applied to label BSA by reacting the –N=C=S group of R-CQDs with the primary NH_2 group of the lysine residue of BSA. Such labeling led to an increase in the fluorescence intensity of R-CQDs and a decrease in that of BSA due to a FRET between BSA and R-CQDs. The apparent dissociation constant (K'_d) and the Hill coefficient are 1.35×10^{-2} mg mL^{-1} and 1.05, respectively, while the binding constant (K) and the number of binding sites are 3.98×10^2 and 1.35, respectively. In addition, the labeling of R-CQDs with BSA follows a pseudo-second order kinetic model with a rate constant (k) of 0.0796 h^{-1} and a maximum labeling efficiency of 31.22%. By adopting this labeling method, the R-CQDs can also be applied for quantification of proteins and an excellent linearity between the fluorescence intensity and the BSA concentration is achieved with an LOD of 7.0 μg mL^{-1}. Since the R-CQDs also displayed a significant photothermal effect with a PCE of up to 60.6% under 808 nm irradiation, the developed labeling technique has the potential to realize an integration of optical diagnosis and photothermal therapy. Compared with the existing CQD labeling methods, our work demonstrates a significant importance in the biochemical field, and it is promising that the as-prepared R-CQDs can be translated into clinical application. However, before it is put into practical use, two potential challenges have to be addressed. First, the lack of long-term cytotoxicity data severely hinders its clinical translation. All the reported cytotoxicity results at present are short-term and cannot provide enough support. Second, the CQDs' *in vivo* accumulation and the resulting impact on healthy tissues and cells remain unknown.

Author contributions

Wanqing Li: methodology, validation, formal analysis, and writing – original draft. Xue Chen: methodology, data curation, and formal analysis. Xipeng Dong: investigation, formal ana-

lysis, and visualization. Zizhuo Zhai: formal analysis and investigation. Yu Kang: formal analysis. Pudun Zhang: conceptualization, methodology, writing – review & editing, supervision, and investigation.

Data availability

The data supporting this article have been included as part of the ESI.†

Conflicts of interest

The authors declare no competing financial interests.

Acknowledgements

The authors are grateful to Prof. Leyu Wang and Prof. Chang Guo for photothermal measurements.

References

1 K. L. Holmes and L. M. Lantz, Chapter 9: Protein labeling with fluorescent probes, in *Method Cell Biol*, 2001, vol. 63, pp. 185–204.
2 C. R. Jing and V. W. Cornish, Chemical tags for labeling proteins inside living cells, *Acc. Chem. Res.*, 2011, **44**(9), 784–792.
3 Y. Kim, S. O. Ho, N. R. Gassman, Y. Korlann, E. V. Landorf, F. R. Collart and S. Weiss, Efficient site-specific labeling of proteins via cysteines, *Bioconjugate Chem.*, 2008, **19**(3), 786–791.
4 M. Rashidian, J. K. Dozier and M. D. Distefano, Enzymatic labeling of proteins: Techniques and approaches, *Bioconjugate Chem.*, 2013, **24**(8), 1277–1294.
5 C. Q. Ding, A. W. Zhu and Y. Tian, Functional surface engineering of C-Dots for fluorescent biosensing and in vivo Bioimaging, *Acc. Chem. Res.*, 2013, **47**(1), 20–30.
6 P. L. Gao, Z. G. Xie and M. Zheng, Small nanoparticles bring big prospect: The synthesis, modification photoluminescence and sensing applications of carbon dots, *Chin. Chem. Lett.*, 2022, **33**(4), 1659–1672.
7 H. X. Qi, Z. Z. Zhai, X. P. Dong and P. D. Zhang, Nitrogen doped carbon quantum dots (N-CQDs) with high luminescence for sensitive and selective detection of hypochlorite ions by fluorescence quenching, *Spectrochim. Acta, Part A*, 2022, **279**, 121456.
8 M. Maruthapandi, A. Durairaj, A. Saravanan, J. H. T. Luong, A. Bakandritsos, A. Gedanken and R. Zboril, The innovative design of carbon dots on polymer texture for highly selective detection of amino compounds, *Carbon*, 2024, **228**, 119414.
9 Y. A. B. Jardan, A. M. Mostafa, J. Barker, A. B. H. Ali and M. M. El-Wekil, A novel route for fabrication of yellow emissive carbon dots for selective and sensitive detection of vitamin B12, *Anal. Methods*, 2025, **17**, 3007.
10 Y. A. B. Jardan, M. M. El-Wekil, A. M. Mostafa, J. Barker and A. B. H. Ali, Dual-emission ratiometric fluorometric platform using Cu@NCDs/eosin system for sensitive detection of metformin: Pharmacokinetic studies in normal and disease states, *Microchem. J.*, 2025, **209**, 112789.
11 S. Singh, K. Dev, S. Bhardwaj, D. Ramakanth, K. R. Singh, K. M. Poluri, K. Ghosh and P. K. Maji, Biodegradable cellulose nanocrystal composites doped with carbon dots for packaging and anticounterfeiting applications, *Nanoscale*, 2025, **17**, 904.
12 J. X. Yang, Q. W. Tang, Q. Meng, Z. F. Zhang, J. Y. Li, B. L. He and P. Z. Yang, Photoelectric conversion beyond sunny days: all weather carbon quantum dot solar cells, *J. Mater. Chem. A*, 2017, **5**(5), 2143–2150.
13 Z. Sheffield, M. Alafeef, P. Moitra, P. Ray and D. Pan, N-gene-complementary antisense-oligonucleotide directed molecular aggregation of dual-colour carbon dots, leading to efficient fluorometric sensing of SARS-COV-2 RNA, *Nanoscale*, 2022, **14**, 5112.
14 A. M. B. H. Ali, M. R. El-Wekil, M. R. Elmasry, Y. A. B. Jardan and M. M. El-Wekil, Engineering a pH-responsive fluorometric system: Dual-emission carbon dots and BTB for selective urea sensing, *J. Photochem. Photobiol., A*, 2025, **466**, 116416.
15 A. M. B. H. Ali, M. R. Elmasry, Y. A. B. Jardan and M. M. El-Wekil, Smart fluorometric sensing of metal contaminants in canned foods: a carbon dot-based dual-response system for quantifying aluminum and cobalt ions, *RSC Adv.*, 2025, **15**, 6962.
16 Z. Q. Wang, Y. Wang, W. T. Li, S. Y. Liu, L. Zhang, J. N. Yang, C. X. Feng, R. F. Chong and Y. M. Zhou, Integrating carbon quantum dots with oxygen vacancy modified nickel-based metal organic frameworks for photocatalytic CO2 reduction to CH4 with approximately 100% selectivity, *J. Colloid Interface Sci.*, 2025, **678**, 689–702.
17 P. Fathi, P. Moitra, M. M. McDonald, M. B. Esch and D. Pan, Near-infrared emitting dual-stimuli-responsive carbon dots from endogenous bile pigments, *Nanoscale*, 2021, **13**, 13487.
18 H. He, D. Liu, Z. Z. Feng, A. J. Guo, L. H. Liu and X. L. Chen, Antifade carbon dots on a plasmonic substrate for enhanced protein detection in immunotherapy, *ACS Sens.*, 2020, **5**(12), 4027–4034.
19 L. M. Wang, J. Wu, B. Z. Wang, G. C. Xing and S. N. Qu, D-arginine-functionalized carbon dots with enhanced near-infrared emission and prolonged metabolism time for tumor fluorescent-guided photothermal therapy, *J. Colloid Interface Sci.*, 2025, **678**, 575–582.
20 O. U. Akakuru, J. Xing, S. Q. Huang, Z. M. Iqbal, S. Bryant, A. Wu and M. Trifkovic, Leveraging non-radiative transitions in asphaltenes-derived carbon dots for cancer photothermal therapy, *Small*, 2024, 2404591.
21 T. Yuan, F. L. Yuan, L. Z. Sui, Y. Zhang, Y. C. Li, X. H. Li, Z. A. Tan and L. Z. Fan, Carbon quantum dots with near-

unity quantum yield bandgap emission for electroluminescent light-emitting diodes, *Angew. Chem., Int. Ed.*, 2023, **62**(20), e202218568.

22 C. X. Wu, S. N. Zhang, M. D. Liu and J. H. He, One-step solvothermal synthesis of nitrogen-doped carbon dots with efficient red emission from conjugated perylene for multiple applications, *Carbon*, 2024, **230**, 119601.

23 T. G. Millan, J. R. Soriano, M. Ghirardello, X. Liu, C. M. Santi, J. C. Eloi, N. Pridmore, R. L. Harniman, D. J. Morgan, S. Hughes, S. A. Davis, T. A. A. Oliver, K. M. Kurian and M. C. Galan, Multicolor Photoluminescent Carbon Dots à La Carte for Biomedical Applications, *ACS Appl. Mater. Interfaces*, 2023, **15**(38), 44711–44721.

24 N. A. Pechnikova, K. Domvri, K. Porpodis, M. S. Istomina, A. V. Iaremenko and A. V. Yaremenko, Carbon quantum dots in biomedical applications: Advances, challenges, and future prospects, *Aggregate*, 2024, e707.

25 H. J. Jian, J. T. Yu, Y. J. Li, B. Unnikrishnan, Y. F. Huang, L. J. Luo, D. H. K. Ma, S. G. Harroun, H. T. Chang, H. J. Lin, J. Y. Lai and C. C. Huang, Highly adhesive carbon quantum dots from biogenic amines for prevention of biofilm formation, *Chem. Eng. J.*, 2020, **386**, 123913.

26 S. M. ElMorsy, D. A. Gutierrez, S. Valdez, J. Kumar, R. Aguilera, M. Noufal, H. Sarma, S. Chinnam and M. Narayan, Graphene acid quantum dots: A highly active multifunctional carbon nano material that intervene in the trajectory towards neurodegeneration, *J. Colloid Interface Sci.*, 2024, **670**, 357–363.

27 S. H. Li, Z. L. Peng and R. M. Leblanc, Method to determine protein concentration in the protein–nanoparticle conjugates aqueous solution using circular dichroism spectroscopy, *Anal. Chem.*, 2015, **87**(13), 6455–6459.

28 R. S. A. Sonthanasamy, N. M. N. Sulaiman, L. L. Tan and A. M. Lazim, Comprehensive spectroscopic studies of synergism between Gadong starch based carbon dots and bovine serum albumin, *Spectrochim. Acta, Part A*, 2019, **218**, 85–96.

29 Y. Behzadipour and S. Hemmati, Covalent conjugation and non-covalent complexation strategies for intracellular delivery of proteins using cell-penetrating peptides, *Biomed. Pharmacother.*, 2024, **176**, 116910.

30 P. P. Liu, C. C. Zhang, X. Liu and P. Cui, Preparation of carbon quantum dots with a high quantum yield and the application in labeling bovine serum albumin, *Appl. Surf. Sci.*, 2016, **368**, 122–128.

31 C. Rao, S. Khan, N. C. Verma and C. K. Nandi, Labelling Proteins with Carbon Nanodots, *ChemBioChem*, 2017, **18**(24), 2385–2389.

32 M. Yazdani, M. Rahmandoust and H. Kouchakzadeh, Development of various carbon nanoparticles and albumin complexes for potential theranostics applications, *J. Drug Delivery Sci. Technol.*, 2022, **77**, 103901.

33 M. H. Tang, P. Teng, Y. J. Long, X. L. Wang, L. P. Liang, D. J. Shen, J. Wang and H. Z. Zheng, Hollow carbon dots labeled with FITC or TRITC for use in fluorescent cellular imaging, *Microchim. Acta*, 2018, **185**, 223.

34 S. Sun, L. Zhang, K. Jiang, A. G. Wu and H. W. Lin, Toward high-efficient red emissive carbon dots: Facile preparation, unique properties, and applications as multifunctional theranostic agents, *Chem. Mater.*, 2016, **28**(23), 8659–8668.

35 Y. Y. Wu, P. Wei, S. Pengpumkiat, E. A. Schumacher and V. T. Remcho, Development of a carbon dot (C-Dot)-linked immunosorbent assay for the detection of human α–Fetoprotein, *Anal. Chem.*, 2015, **87**(16), 8510–8516.

36 N. Barbero, C. Barolo and G. Viscardi, Bovine serum albumin bioconjugation with FITC, *World J. Chem. Educ.*, 2016, **4**(4), 80–85.

37 D. Qu, Z. C. Sun, M. Zheng, J. Li, Y. Q. Zhang, G. Q. Zhang, H. F. Zhao, X. Y. Liu and Z. G. Xie, Three colors emission from S,N Co-doped graphene quantum dots for visible light H_2 production and bioimaging, *Adv. Opt. Mater.*, 2015, **3**(3), 360–367.

38 Y. Yuan, L. L. Wu, B. B. Yan, Y. Y. Yu, Q. Wang and P. Wang, Fabrication and efficient interfacial assembly of bright red-emitting carbon quantum dots for security-warning textiles, *Small*, 2024, **20**(45), 2405101.

39 Y. J. Zhao, L. X. Yu, Y. K. Deng, K. L. Peng, Y. Yu and X. L. Zeng, A multi-color carbon quantum dots based on the coordinated effect of quantum size and surface defects with green synthesis, *Ceram. Int.*, 2023, **49**(11), 16647–16651.

40 B. Y. Wang, J. K. Yu, L. Z. Sui, S. J. Zhu, Z. Y. Tang, B. Yang and S. Y. Lu, Rational design of multi-color-emissive carbon dots in a single reaction system by hydrothermal, *Adv. Sci.*, 2021, **8**, 2001453.

41 Z. Z. Zhai, X. P. Dong, H. X. Qi, R. T. Tao and P. D. Zhang, Carbon quantum dots with high photothermal conversion efficiency and their application in photothermal modulated reversible deformation of poly(N-isopropylacrylamide) hydrogel, *ACS Appl. Bio Mater.*, 2023, **6**(9), 3395–3405.

42 H. Wang, R. J. Zhang, D. Yuan, S. Y. Xu and L. Y. Wang, Gas foaming guided fabrication of 3D porous plasmonic nanoplatform with broadband absorption, tunable shape, excellent stability, and high photothermal efficiency for solar water purification, *Adv. Funct. Mater.*, 2020, **30**(46), 2003995.

43 Y. Yuan, X. M. Bao, L. L. Wu, M. Zhou, Y. Y. Yu, Q. Wang and P. Wang, Solvent-regulated synthesis of full-color fluorescent nitrogen/sulfur co-doped carbon quantum dots for anti-counterfeiting textiles, *Chem. Eng. J.*, 2024, **493**, 152488.

44 X. P. Dong, W. Q. Li, X. Chen, E. Zhuo, Z. Z. Zhai, H. X. Qi, Y. Kang and P. D. Zhang, Ethylenediamine assisted synthesis of o-Phenylenediamine-Based red emissive carbon quantum dots: A strategy to improve the fluorescence quantum yield, *Adv. Opt. Mater.*, 2025, **13**(3), 2402173.

45 S. H. Qu, F. Y. Sun, Z. H. Qiao, J. M. Li and L. Shang, In situ investigation on the protein corona formation of quantum dots by using fluorescence resonance energy transfer, *Small*, 2020, **16**(21), 1907633.

46 B. I. Kurganov, A. V. Lobanov, I. A. Borisov and A. N. Reshetilov, Criterion for Hill equation validity for

description of biosensor calibration curves, *Anal. Chim. Acta*, 2001, **427**(1), 11–19.
47 S. Goutelle, M. Maurin, F. Rougier, X. Barbaut, L. Bourguignon, M. Ducher and P. Maire, The Hill equation: a review of its capabilities in pharmacological modelling, *Fundam. Clin. Pharmacol.*, 2008, **22**(6), 633–648.
48 P. D. Pino, B. Pelaz, Q. Zhang, P. Maffre, G. U. Nienhaus and W. J. Parak, Protein corona formation around nanoparticles-from the past to the future, *Mater. Horiz.*, 2014, **1**(3), 301–313.
49 P. Szymaszek, P. Fiedor, A. C. Brekiesz, M. T. Czochara, T. Swiergosz and J. Ortyl, Molecular interactions of bovine serum albumin (BSA) with pyridine derivatives as candidates for non-covalent protein probes: a spectroscopic investigation, *J. Mol. Liq.*, 2022, **347**, 118262.